

# Scaling Limits of Free-Space Tilt Mirror MEMS Switches for Data Center Networks

William M. Mellette and Joseph E. Ford

Department of Electrical & Computer Engineering, University of California San Diego, 9500 Gilman Drive, La Jolla, California, 92093

Author e-mail address: wmellett@ucsd.edu

**Abstract:** We present a first-principles analysis of the scaling of switch response speed as a function of port count, crosstalk, and insertion loss, based on physical optics and kinematics of canonical MEMS tilt mirror switch structures.

**OCIS codes:** (130.4815) Optical switching devices; (230.4685) Optical microelectromechanical devices

## 1. Introduction

High-speed optical circuit switches (OCS) have recently been proposed for data center networks to provide reconfigurable high-bandwidth and data-rate agnostic channels without cascaded optical transceivers [1]. Free-space optical microelectromechanical systems (MEMS) crossconnects and wavelength add/drop switches permeate telecommunication networks [2, 3], where bandwidth provisioning and protection requires 10-100ms response times. Digital MEMS tilt mirrors can switch in 20 microseconds or less [4, 5], but have found limited use in telecom switches which are typically optimized for port count and efficiency. In the data center, switching speed and port count are both critical figures of merit. The fraction of traffic that can flow through a data center OCS is directly related to switch reconfiguration rate, and sub-millisecond switches are essential to meet the network demands [6].

Here, we re-examine MEMS tilt mirror devices to quantify the fundamental limits to switching speed. A basic  $1 \times N$  MEMS switch directs light from an input fiber through free space to an electrostatically actuated mirror, which redirects the light to couple to one of the output fibers.  $N \times N$  and multistage switches can be made using free space and relay optics to refocus light between a series of mirrors. While the specifics of switch layouts may differ, the fundamental requirement is that the mirror discriminates between switch states. Using fundamental physical mechanics and free-space optics, we investigate how the response time of canonical one- and two-axis tilt mirror MEMS devices scales as a function of switch port count, crosstalk, and insertion loss.

## 2. Device and System Modeling

Each micromirror is supported by a torsion or deflection spring structure such that it can be tilted by an electrostatic force applied by a set of nearby electrodes. As with any harmonic oscillator, the response time of the mirror is inversely proportional to its resonant frequency, given by  $\omega = \sqrt{k/I}$  where  $k$  is the spring constant of the support springs and  $I$  is the rotational inertia of the structure. While the exact proportionality depends on damping from the surrounding gas, the resonant frequency is a figure of merit for comparing the response speeds of different devices.

The maximum mechanical tilt angle of the mirror determines the maximum angle a beam of light can be steered and is found by balancing the restoring torque of the supporting springs, approximated using Hooke's law, with the electrostatic torque generated by the voltage applied between the electrode and mirror, which acts as the second electrode. Ignoring fringing fields, the electrostatic torque can be found as a function of tilt angle by differentiating the stored energy in the effective capacitor to be  $\tau_{drive}(\theta) = (1/2)\epsilon_0 V^2 \partial(A/d)/\partial\theta$ , where  $\epsilon_0$  is the vacuum permittivity,  $V$  is the applied voltage,  $\theta$  is the mechanical tilt angle of the mirror,  $A$  is the area of overlap between the electrodes, and  $d$  is the distance between the electrodes. We limited the applied voltage to 275V to avoid electrostatic breakdown. Despite the high operating voltage, with appropriate drive electronics the device can have low power dissipation because the electrostatic operating current is relatively small.

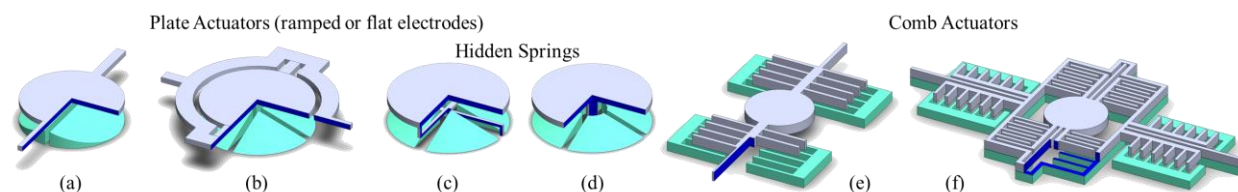


Fig. 1. Device geometries considered: (a) 1-axis plate, (b) 2-axis plate with gimbal, (c) 2-axis plate with hidden crossbar springs, (d) 2-axis plate with hidden post, (e) 1-axis comb, and (f) 2-axis comb. The plate drives are shown with ramped electrodes, but were also analyzed with flat parallel plate electrodes. Electrodes are cyan colored.

The functionality of  $A$  and  $d$  with respect to  $\theta$  as well as the rotational inertia  $I$  are determined by the drive mechanism. In our analysis, we consider vertically offset comb, parallel (flat) plate, and ramped plate drive mechanisms [7] [Fig. 1]. The plate drive is a gap closing actuator and experiences the well-known “pull-in” phenomenon where the mirror is snapped down to the substrate, at about 44% of the maximum tilt angle, when the nonlinearity in the driving torque overcomes the linear restoring torque. One can purposely drive the device to pull-in [4, 5] and operate in a “digital” manner between a discrete number of mirror positions. The plate drive can also be operated in an “analog” regime where pull-in is avoided, allowing a continuous range of mirror positions over a smaller angular range. Under analog operation, the resonant frequency of the mirror is a function of tilt angle and approaches zero at the pull-in angle. The comb drive, an area-increasing actuator, does not experience pull-in and operates in a continuous analog fashion.

In order to determine the port count  $N$  of the switch, we must determine the number of resolvable signal beams  $M$  contained within the angular tilting range of each mirror. We model the propagation of light in free space as a Gaussian beam parameterized by a waist  $w_0$  and wavelength  $\lambda$  (set at 1550nm). Because a Gaussian beam is infinite in spatial extent, the beam is necessarily clipped at each mirror, resulting in a loss of power and diffraction from the mirror edges. The spatial confinement efficiency  $\eta_{sc}$  is the fraction of power encircled by the mirror, given by  $\eta_{sc} = 1 - \exp(-2r_m^2/w_0^2)$ , where  $r_m$  is the mirror radius. The far-field diffraction pattern is found by convolving the Fourier transforms of the Gaussian field and the mirror aperture. For a desired angular confinement efficiency, the beam divergence  $\beta$  [Fig. 2(b)] can be found by calculating the far field on-axis encircled energy [Fig. 2(c)]. Crosstalk with adjacent ports can be found by integrating off-axis encircled energy [Fig. 2(d)].

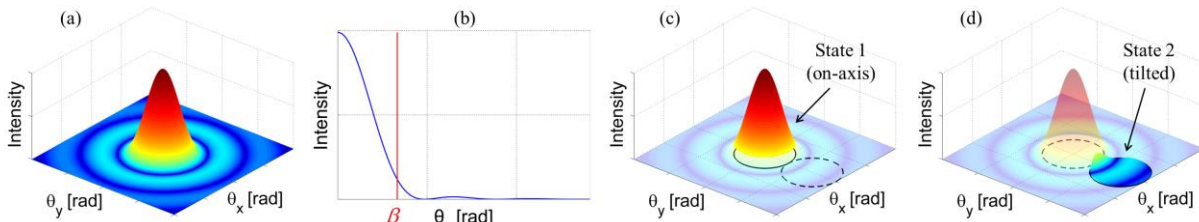


Fig. 2. (a) Far field diffraction pattern. (b) Variable definition of beam divergence. (c) On-axis encircled energy. (d) Off-axis encircled energy.

In one dimension, for small tilt angles, the number of resolvable beams is  $M_1 = \alpha(2\theta_{\max} / \beta + 1)$ , where  $2\theta_{\max}$  is the full mechanical tilt range and  $\alpha$  is the fill factor of the mirrors, taking into account any springs, combs, and gimbal structures. For small angles, the two-axis comb drive traces a rectangle in angular space and can resolve  $M_2 = M_{1x}M_{1y}$  beams where  $M_{1x}$  and  $M_{1y}$  are the number of one dimensional resolvable beams along each axis. The two-axis plate drive traces an ellipse in angular space and can resolve  $M_2 = \pi M_{1x}M_{1y} / 4$  beams.

The number of ports  $N$  in the switch can be calculated by defining a topology that uses a number of  $M$  - state mirror devices. The total throughput efficiency  $\eta_t$  for an  $S$  - stage switch is given by  $\eta_t = \eta_f (\eta_{sc}\eta_{ac}R)^S$ , where  $\eta_f$  is the fiber coupling efficiency (assumed to be 90%),  $\eta_{sc}$  is the spatial confinement efficiency,  $\eta_{ac}$  is the angular confinement efficiency, and  $R$  is the mirror reflectivity (assumed to be 97% for gold at 1550nm). A  $1 \times N$  port switch can be constructed from an  $S = \log_M(N)$  stage  $M$ -ary tree, using a total of  $(N-1)/(M-1)$  mirrors. Similarly, an  $N \times N$  port switch can be constructed from an  $S = 2\log_M(N)$  stage folded  $M$ -ary tree, using  $2N(N-1)/(M-1)$  mirrors. In this framework, a 2-stage  $N \times N$  switch represents a conventional z-fold optical cross connect (OXC).

### 3. Simulation and Results

We constructed a numerical model in Matlab to calculate the resonant frequency  $\omega$  and number of resolvable beams  $M$  for each MEMS device given a set of parameters which define the geometrical form of the structure. We defined limits to the form for each device based on realistic fabrication constraints and calculated the performance of devices within this space. Care was taken to insure that the input parameters were finely discretized and had appropriate boundaries in order to ensure convergence and to avoid over-restriction of the design space. We sorted the designs in terms of resonant frequency to find the design with the fastest response for a specified insertion loss, crosstalk, and port count. Figure 3(a) shows the resonant frequency as a function of port count for a 2-stage  $N \times N$  switch using the one-axis MEMS devices, constraining insertion loss to be better than 3dB and nearest neighbor crosstalk to be better than -20dB. Figure 3(b) shows the same for the two-axis MEMS devices.

Examining the performance of the one-axis designs, we see that for a 2 port switch, the plate drive is nearly an order of magnitude faster when operated in digital mode rather than analog mode. This is because the analog operating regime imposes a lower resonant frequency and a smaller tilt angle to avoid pull-in, and because digital operation benefits from the increased tilting range acquired by allowing the mirror to make contact with the

substrate. The comb drive is slower than the plate drive when  $N$  is small because the comb fingers add significant inertia. As we increase  $N$ , the mirror must necessarily get larger as a consequence of diffraction. In this regime, the comb drive surpasses the plate drive as the inertial contribution of the comb fingers relative to the mirror decreases. The ramped electrodes have a more significant improvement in one-axis plate drives than in two-axis designs.

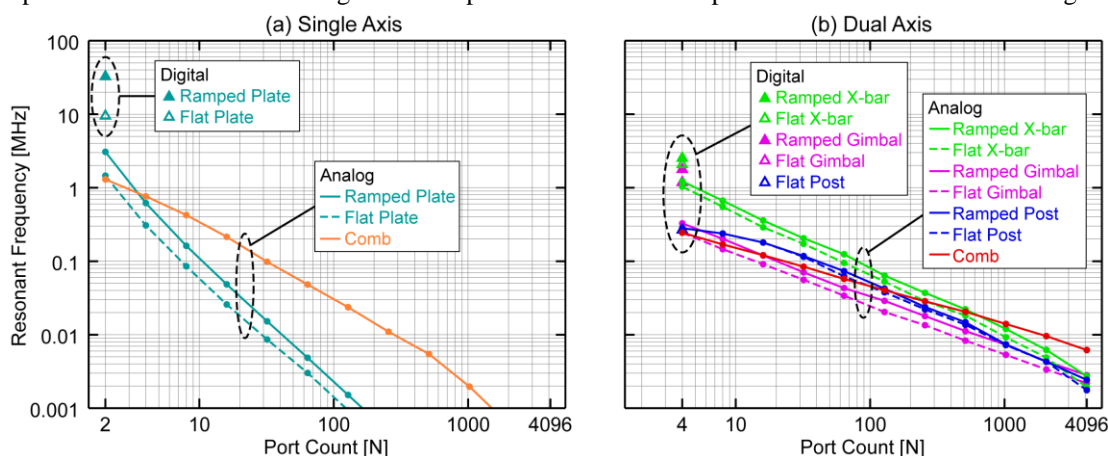


Fig. 3. Resonant frequency as a function of port count for a 2-stage  $N \times N$  switch using (a) 1-axis and (b) 2-axis MEMS tilt mirrors. Filled triangles and solid lines indicate ramped electrodes, while hollow triangles and dashed lines represent flat electrodes for the plate drive.

In the two-axis designs, we again see that operating in the digital regime allows faster response times for the same reasons outlined above. In the limit of small  $N$ , both the comb and gimbaled plate drives suffer from a larger inertial impact of the gimbal structure compared to the gimbal-less hidden crossbar design. However, as the size of the mirror scales with  $N$ , the inertial contribution from the offset between center of mass and rotation axes for the gimbal-less design increases while the fractional inertial contribution of the gimbal relative to the mirror decreases. Despite its lower fill factor, the two-axis comb drive enables the fastest switching speeds in the high port count limit.

Weighting reconfiguration speed and number of ports equally, we can define a performance metric as the number of reconfigurable ports per unit time, computed as the product of the resonant frequency and port count. We find that the one-axis plate drive operating in the digital regime maximizes this metric with  $6.5 \times 10^7$  reconfigurable ports per second despite only having 2 ports. At the opposite extreme in terms of port count and speed, the two-axis comb drive has the second highest metric with  $2.8 \times 10^7$  reconfigurable ports per second for a 4096 port switch.

#### 4. Switch Design

This analysis provides a useful tool for evaluating the design trade space. We investigated the tradeoff between optical performance parameters (crosstalk and insertion loss) for increasing switch speed, and concluded that significant increases in switch speed cannot be achieved by any reasonable sacrifice in optical performance; for example, a 10x increase in speed requires a 30dB increase in loss. This indicates we need new overall optical configurations to achieve microsecond-scale switching with the large port count necessary for data center optical circuit switching. We have investigated two new switch designs with more favorable scaling properties than a two-stage OXC. One is a multiport wavelength selective switch which leverages the high reconfiguration speed of one-axis digital MEMS mirrors in conjunction with relay optics to enable larger port count. The other uses freespace optics to interconnect a number of small port count OXCs in a Clos network to achieve larger port count, leveraging the fact that switches with fewer ports switch at a faster rate. Although space constraints limit their inclusion here, we will discuss the details of these optical designs and their performance in the conference presentation.

*This work is supported by the National Science Foundation under grant #1314921.*

#### References

- [1] N. Farrington, G. Porter, S. Radhakrishnan, H. Bazzaz, V. Subramanya, Y. Fainman, G. Papen, and A. Vahdat, "Helios: A Hybrid Electrical/Optical Switch Architecture for Modular Data Centers," in Proc. ACM SIGCOMM, 2010, pp. 339-350.
- [2] M. Wu, O. Solgaard, and J. Ford, "Optical MEMS for Lightwave Communication," J. Lightwave Tech., **24**(12), 4433-4454 (2006).
- [3] J. Kim et. al., "1100 x 1100 Port MEMS-Based Optical Crossconnect With 4-dB Maximum Loss," IEEE Photonics Tech. Lett., **15**(11), 1537-1539 (2003).
- [4] J. E. Ford et. al., "Wavelength add/drop switching using tilting micromirrors," IEEE J. Lightwave Tech., **17**(5), 904-911 (1999).
- [5] R. Knipe, "Challenges of a Digital Micromirror Device: modeling and design," in Proc. SPIE 2783, Micro-Optical Technologies for Measurement, Sensors, and Microsystems, 1996, pp. 135-145.
- [6] G. Porter et. al., "Integrating microsecond circuit switching into the data center," in Proc. ACM SIGCOMM, 2013, pp. 447-458.
- [7] J. Tsai and M. Wu, "Gimbal-Less MEMS Two-Axis Optical Scanner Array With High Fill-Factor," J. Microelectromechanical Systems, **14**(6), 1323-1328 (2005).